Molecular Cell, Volume *30*

Supplemental Data

Transient Reversal of RNA Polymerase II Active Site Closing Controls Fidelity of Transcription Elongation

Maria L. Kireeva, Yuri A. Nedialkov, Gina H. Cremona, Yuri A. Purtov, Lucyna Lubkowska, Francisco Malagon, Zachary F. Burton, Jeffrey N. Strathern, and Mikhail Kashlev

Supplementary Material (Kireeva *et al*.)

Assays for the translocation state of the TEC

Exonuclease III (Exo III) footprinting is established as a reliable tool for mapping the positions of stalled elongation complexes on double-strand DNA templates and for understanding the dynamics of RNA polymerases during transcription elongation, pausing and arrest (Landick and Yanofsky, 1987; Metzger et al., 1989; Nudler et al., 1994; Samkurashvili and Luse, 1996; Komissarova and Kashlev, 1998). Lately, the frequently observed heterogeneity of the polymerase boundaries detected by Exo III have been interpreted as evidence of different translocation states of the TEC (Artsimovitch et al., 2003; Bar-Nahum et al., 2005; Kashkina et al., 2006). We believe, however, that the heterogeneity of the enzyme boundaries does not necessarily reflect the state of equilibrium between the pre- and post-translocation TECs. Here we describe the modifications that we introduced to the Exo III footprinting technique to ensure that this technique can be applied to the analyses of Pol II translocation. We also discuss the remaining limitations of this assay which should be taken into account for the interpretation of the Exo III footprinting results, as well as other methods that could be used to determine the translocation state of the TEC.

1. Limiting the backtracking by minimizing the RNA length. Exo III footprinting of bacterial and eukaryotic TECs revealed lateral mobility (reversible backtracking) of RNA polymerases by showing heterogeneity of the TEC boundaries on DNA (multiple sites of the Exo III stopping) (Samkurashvili and Luse, 1996; Komissarova and Kashlev, 1997). Backtracking may mask the pre- and post-translocation positions of the polymerase by generating multiple front- and rear-end boundaries of the TEC as observed previously (Bar-Nahum et al., 2005). Therefore, to determine the effect of mutation in the Pol II Rpb1 subunit on translocation, we used laterally stable TECs carrying 8-11-nt RNA, which resisted backtracking due to the short length of their transcripts. As we expected, for all the TECs tested only two upstream boundaries, located 15 bp and 16 bp from the 3'-end of the RNA, appear on template DNA strand footprints (Fig. 4 and Supplementary Fig. 5, 6B, 7A). No new boundary was detected after

prolonged incubation with Exo III. We attribute these two boundaries to the post-translocated and pre-translocated states of the TEC, rather than other conformational changes or a reversible scrunching of the upstream DNA by the RNA polymerase (Guo and Sousa, 2006). This conclusion was based on the similar response of the rear and the front-end boundaries of the enzyme to the addition of the incoming NTP or incorporation of a 3'dNTP (Fig. 4C and Supplementary Fig. 4). The rear-end boundaries of all TECs analyzed in this work were detected as two distinct bands (Fig. 4). In contrast, the front-end boundary of TEC9, assembled on TDS65 and labeled NDS65 (Supplementary Table; note that NDS65 used in this experiment was not biotinylated; see part 2 for details), consisted of several bands which moved two bp downstream after formation of TEC11 (Supplementary Fig. 4A, compare lanes 3, 4 and 6, 7). The multiple front end boundaries of TECs halted at unique template positions were reported previously (Toulokhonov et al., 2007). This intrinsic property of the interactions of RNA Pol II with the downstream DNA hindered an accurate identification of the pre- and post-translocated states of the enzyme by digestion with Exo III. The rear-end boundary of TEC11 was shifted toward the upstream position when the AMP at the 3'-end of the RNA was substituted with the terminating 3'dAMP the complexes. This characteristic shift was similar to the movement of the TECs presented in Fig. 4 (compare lanes 2-3 and 5-6 in Supplementary Fig. 4B). Addition of CTP to the 3'dA-terminated TEC11 caused the downstream shift of the front-end boundary (compare lanes 6 and 9 in Supplementary Fig. 4B). The similar response of both boundaries of the enzyme to the incoming NTP and to incorporation of 3'dNMP supports the idea that these footprints correspond to the pre- and post-translocation equilibrium of RNAP.

2. Rear-end footprinting and blocking of the opposite DNA strand degradation. The susceptibility of Pol II to backtracking may result in the induction of the backward translocation by Exo III approaching the front end of the TEC and "pushing" it backwards. To avoid this potential artifact, we blocked degradation of the non-template DNA strand by biotinylation of its 3'-end and analyzed the footprints of Pol II on the template DNA. A similar approach for the elimination of pushing activity of Exo III was recently reported (Toulokhonov et al., 2007).

3. Control for melting of upstream DNA. Exonuclease III is a 3'->5' exonuclease degrading only duplex DNA. Therefore, the approach of Exo III to RNA polymerase may be stopped not only by collision with Pol II, but also by melting the remaining short double-strand DNA fragment upstream from the elongation complex. Indeed, the 15-nt distance of the rear-end Pol II boundary from the 3'-end of the RNA, taken together with the minimal stable 8-bp length of the RNA-DNA hybrid and 10-12-nt size of the transcription bubble, leave only 4-7 bp of the dsDNA in the TEC treated with Exo III. To test whether the spontaneous melting of the upstream DNA duplex in a course of digestion with Exo III was a factor in determining the size of the footprint, we tested the temperature dependence of the footprint position (Supplementary Fig. 5). If the DNA melting has an impact on the Exo III activity, an additional advancement of Exo III at a lower temperature and/or premature stopping of Exo III at a higher temperature could be expected. However, the result of the experiment ruled out the impact of the dsDNA melting on DNA shortening by Exo III: in the two different TECs tested in the experiment, the position of the boundaries was not temperature-dependent. The degradation of the DNA occurred slowly at 15°C, and it was accelerated upon the increase of the reaction temperature. This pattern indicated that the short DNA duplex sustained in TECs treated with Exo III.

4. The sequence specificity of Exo III and comparison of different TECs. The conclusion about the translocation state of the TEC is commonly drawn from the distribution of multiple boundaries of the TEC, observed at one time point (presumably taken before the DNA is degraded to the shortest product possible). To account for the translocation state, this distribution should change (the boundary should move in the direction of transcription) in response to the addition of the next NTP, the incorporation of which is blocked (Artsimovitch et al., 2003; Bar-Nahum et al., 2005; Toulokhonov et al., 2007). In addition to the analysis of the boundaries distribution at a single time point, we found it necessary to observe the dynamics of the appearance of the Pol II boundaries in the same TEC in the course of incubation with Exo III. This requirement is connected with the sequence specificity of Exo III, with dCMP being cleaved off most efficiently (Linxweiler and Horz, 1982).

For example, for TEC9 and TEC10 formed with WT Pol II on TDS/NDS65 template, the boundary attributed to the pre-translocated TEC (16 nt upstream from the RNA 3'-end) appears after 20 sec of incubation with Exo III in standard conditions (25° C, 3.3 units/μl). Its conversion to the post-translocated boundary occurs slowly, with the equal distribution observed at approximately 2 min (Fig. 4B, C). In contrast to the TEC9, the post-translocated boundary of TEC10 becomes predominant after less than 1 min incubation with Exo III. This result could indicate that TEC9 is predominantly pre-translocated and TEC10 is predominantly post-translocated. However, this conclusion contradicts the results of the pyrophosphorolysis test. TEC10 undergoes rapid pyrophosphorolysis, while in a fraction of TEC9 the RNA is shortened relatively slowly (Supplementary Fig. 6A). Representing reversal of NTP incorporation into the nascent transcript, the pyrophosphorolysis occurs in the pre-translocated TECs. Therefore, the time-course of pyrophosphorolysis suggests that TEC10 is mostly pre-translocated, while TEC9 has two approximately equal fractions representing the pre-and post-translocated states. The contradiction between the results of the Exo III footprinting and the pyrophosphorolysis assay could be explained by a significantly slower degradation of the DNA by Exo III in the post-translocated TEC9, as compared to the post-translocated TEC10. Indeed, in the case of TEC10, the conversion of the pre-translocated boundary to the post-translocated one involves cleaving off the dCMP residue, which is the preferred substrate for Exo III (Linxweiler and Horz, 1982). When TEC8, TEC9, and TEC10 were obtained on the template carrying a stretch of five consecutive dCMP residues in the upstream region of the template DNA strand, the apparent post-translocated fraction increased in TEC8 and TEC9 (compare Supplementary Fig. 6B and Fig. 4B and C in the main text), but did not change in TEC10 (Supplementary Fig. 5 and 6B). Elimination of the sequence-specific inhibition of Exo III digestion resolved the contradiction between the two tests addressing the translocation state of the TECs.

Taken together, the dynamics of the pyrophosphate-induced RNA degradation (supplementary Fig. 6A) and the time-course of the post-translocated boundary accumulation (Supplementary Fig. 6B) suggest that WT TEC8 is predominantly post-translocated whereas TEC9 is distributed between the pre- and post-translocated states. By this standard TEC10 is mostly pre-translocated. The placement of an

oligo-dC stretch in the template DNA strand region located 15-16 nt upstream from the 3'-ends of the RNAs in the TECs being analyzed allowed us to use Exo III footprinting to compare the translocation of the TECs stalled at different positions on the template. Exo III footprinting is the most direct way to analyze the translocation state of the TEC, because, unlike pyrophosphorolysis, the dynamics of the enzyme boundaries distribution detected by Exo III does not depend on the catalytic activity of Pol II. For instance, Exo III footprinting detects a pre-translocated fraction of TEC8 (Supplementary Fig. 6B, the first lane), which is not observed in the pyrophosphorolysis assay (Supplementary Fig. 6A), most likely due to the inefficiency of the pyrophosphate-induced RNA degradation beyond 8 nucleotides.

Susceptibility of the oligo-dCMP stretch to degradation by Exo III makes Exo III footprinting suitable for a semi-quantitative analysis of the pre- and post-translocated fractions in the stalled TEC. The shortest time points after addition of Exo III give the best approximation of the translocation state of TEC, while the prolonged incubation with Exo III leads to over-estimation of the post-translocated fraction. The shortest time point showing the pre- and post-translocated boundaries in the TEC8 and TEC10 formed on TDS/NDS65C was 5 sec, which is the time required for Exo III to degrade the DNA upstream from RNA polymerase (Supplementary Fig. 7A). At this time point, a significant amount of Exo III has been delayed well upstream of the elongation complex on the dTMP-induced pause sites. In the assembled system, a complete substitution of the non-coding upstream sequence with the homopolymeric dC stretch in the template DNA strand may further improve the quantitative aspect of the Exo III-based assay of the Pol II translocation state.

5. Translocation state of TEC on DNA determined by Exo III footprinting and pre-steady state kinetic analysis using EDTA as a quencher. Another approach to reveal the pre-and post-translocation fractions of the stalled TEC has been proposed based on the pre-steady-state kinetic analyses of mammalian Pol II. It has been suggested that the fast sequestration of the NTP from EDTA occurs only in the TECs that reside in a post-translocated state at the moment of NTP addition (Nedialkov et al., 2003a; Nedialkov et al., 2003b; Zhang and Burton, 2004). The size of the fast fraction in the time course, obtained with the EDTA quench, has been considered indicative of the equilibrium between the pre- and

post-translocation states in the TEC before the addition of NTPs. We explored this correlation for the TECs formed with yeast Pol II. For the WT TEC9, the approximately 50-70% fraction of the post-translocated complexes determined by both Exo III footprinting and pyrophosphorolysis assays (Supplementary Fig. 6), correlates well with the size of the fast fraction in EDTA quench (Fig. 5A, B). However, E1103G mutation delays the transition of the Pol II border from the pre-translocated to the post-translocated position on one hand (Fig. 4 C-E), and, on the other hand, increases the size of the fast fraction in EDTA quench (Fig. 5A, B). To further investigate how the amplitude of the fast fraction observed in EDTA quench correlates with the translocation state determined by Exo III in the WT TECs, we compared Exo III footprints and time-courses of incoming NTP sequestration by TEC8 and TEC10 (Supplementary Fig. 7). According to the Exo III footprinting results, not more than 43% of TEC8 and not more than 14% of TEC10 reside in the post-translocated state, suggesting that the fast fraction of TEC10 in EDTA quench should not exceed 15%, and that the fast fraction of TEC8 in EDTA quench should be about three times greater. However, the fast fraction of the TEC10 was slightly higher, and the fast fraction of TEC8 was significantly lower than expected (Supplementary Fig. 7B). Furthermore, the Exo III footprints of TEC8 and TEC9 suggest that TEC8 is slightly more enriched with the post-translocated complex than TEC9 (Supplementary Fig. 6B). At the same time, the fast fraction of TEC8 (25%) is noticeably smaller than the fast fraction of the TEC9 (50-70%) in EDTA quench (Fig. 7B). Taken together, these results strongly argue against the simple correlation between the fast fraction amplitude in the time-course of NTP incorporation in the EDTA quench setup, and the propensity of the stalled TEC to reside in the post-translocated state. Exo III footprinting emerges as the most direct way to determine the translocation state of the TEC, which does not depend on the catalytic activity of Pol II. Therefore, we relied on this method to assess the effect of E1103G mutation on translocation properties of Pol II.

Kinetic modeling

Our initial biochemical analyses using HCl as a quencher revealed that the kinetics of NTP incorporation by Pol II could be described with a single-exponential equation for both correct and incorrect substrates (Fig. 3). The equation used for the data fit was $y = A\times(1-e^{-kx})$, where y is the fraction of the extended RNA at a given time point, A is the percentage of complexes that extend the RNA at a given rate, k is the reaction rate, x is the time. The A value was more than 80% in all time-courses analyzed. The error in the rate value was less than 10%. The rates obtained for different concentrations of the substrate were fit with the hyperbolic equation $y=k_{pol}\times x/(K_D+x)$, where k_{pol} is the apparent maximum polymerization rate, K_D is the apparent dissociation constant for the NTP, x is the NTP concentration, and y is the apparent reaction rate. The apparent dissociation constants for the complementary and non-complementary substrate are summarized in Table 1.

Global kinetic modeling show that the data for misincorporation fit a two-step mechanism that includes incorrect NTP binding and formation of a phosphodiester bond. According to this mechanism, the increased misincorporation by E1103G Pol II could be attributed to the increase in the rate of bond formation with a non-complementary substrate (Supplementary Fig. 8A). The data for the correct NTP incorporation could be explained by the same kinetic mechanism (data not shown and Supplementary Fig. 8B, HCl quench). The model shown in Supplementary Fig. 8 assumes that the E1103G mutation affects misincorporation rate to a much higher extent than the complementary NTP incorporation rate.

Next, we tested if the results of the EDTA quench also fit the simple two-step mechanism. To model the EDTA quench, we had to first identify the intermediates of the NTP addition reaction that are inactivated by EDTA. The data of Fig. 5 showed that the dilution of the labeled substrate and its inactivation with EDTA resulted in incorporation of essentially the same amount of the labeled substrate into TEC10. This result indicated that EDTA inactivates only a free pool of NTPs without accessing NTP bound to any of the putative binding sites in the protein (A, E, or PS site). We used this important clue to introduce an additional step in our kinetic mechanism (Fig. 5B and Supplementary Fig. 8B) involving

irreversible inactivation of free CTP by EDTA (CTP-Mg^{2+} + EDTA -> CTP + Mg^{2+}-EDTA). Stopping the reaction by EDTA, which sequesters the metal ion, but does not affect the enzyme, requires introduction of two subsequent steps in the reaction: (1) addition of CTP-Mg^{2+} to TEC followed by (2) addition of EDTA to a mixture of TEC-CTP-Mg^{2+} and free CTP-Mg^{2+}, where only free CTP-Mg^{2+} reacts with EDTA. To perform this task we took advantage of the KinTek Global Explorer allowing "multiple mix" option to model subsequent addition of two reactants to the reaction at different time points. The kinetic simulation reveals that the two-step mechanism involving a simple equilibrium between free CTP-Mg^{2+} and CTP-Mg^{2+} bound to TEC does not adequately describe the EDTA quench curves (Supplementary Fig. 8B, the right-side panel). Addition of a reversible isomerization step to the mechanism results in a better fit of EDTA quench data, and allows modeling the difference between the kinetics obtained with the WT and mutant Pol II TECs by changing a single parameter, the rate of the reverse isomerization step (Fig. 5B, C).

It is important to note that not all the rate constants in the suggested mechanisms have been determined experimentally. The pre-steady-state data provide information about the apparent dissociation constant, the apparent NTP incorporation rate (HCl quench), and the apparent isomerization rate (EDTA quench). To estimate k_{+1} and k_{-1} rates of the initial NTP binding, we could rely on the apparent dissociation constants. The initial "on" rate k_{+1} has been assumed the same for the correct and incorrect substrates, which should be the case before any substrate selection takes place. The dissociation rate of non-complementary UTP has been assumed to be faster than other steps in the mechanism (10 000 s^{-1}). k_{+1} for UTP has been calculated as k_{-1}/*apparent* K_D. k_{-1} for the correct CTP has been calculated as $k_{-1} \times$ *apparent* K_D. The 100 s^{-1} CTP dissociation rate is slow compared to the isomerization rate (see below), suggesting that the initially bound complementary NTP is not at a true equilibrium with the free NTP pool. Functionally, this conclusion means that NTP bound to any of multiple pre-loading sites and to the active center is equally protected from EDTA unless it is released from the enzyme. Therefore, because NTP remains in the polymerase during several rounds of isomerization, the apparent K_D could be influenced by the rates of the subsequent steps such as the phosphodiester bond formation. We checked

the model fit at different values of k_{+1} and k_{-1} at multiple CTP concentrations, and found that k_{+1} of 2.5 $\mu M^{-1}s^{-1}$ and k_{-1} of 100 s^{-1} still provide one of the best fits for the HCl and EDTA data. The increase of the binding rate by E1103G mutation could not, without changing the values of other rates, account for the effects of the mutation on the apparent rates of CTP incorporation, CTP sequestration, and UTP misincorporation.

As shown in Supplementary Fig. 8B, the increase of the bond formation rate k_3 alone is not consistent with the EDTA quench data. We did not have to assume that the mutation affects the rate of the catalysis per se. Therefore, k_3 has been set close to the apparent maximum polymerization rate for the mutant. We cannot rule out the possibility that E1103G mutation affects multiple steps in the nucleotide addition cycle. Further pre-steady-state experiments, which would include analysis of two bonds and will be done in a variety of conditions, are required to establish the complete mechanism of transcription elongation and the changes in the mechanism induced by this and other mutations. The sketchy kinetic modeling presented in this work serves as a tool for identification of at least one process, which is impaired by E1103G mutation in Rpb1. We propose the model that contains a minimal number of steps to account for our experimental observations.

The existing models of transcription elongation based on pre-steady-state kinetic analyses of *E.coli* RNA polymerase (Foster et al., 2001; Holmes et al., 2003; Holmes and Erie, 2003) and human Pol II (Zhang et al., 2003; Nedialkov et al., 2003a; Zhang and Burton, 2004; Gong et al., 2005) consider multiple conformations of the TECs, which have distinct affinities to the substrate, and incorporate NTP at different rates. Importantly, the initial analyses that lead to these models have been done using the EDTA quench and multiple conformations have been invoked to explain the biphasic nature of the time courses. Even though it has been later revealed that the dynamics of NTP incorporation in the acid quench dramatically differs from the one observed in EDTA quench (Zhang and Burton, 2004), the above observation itself did not call for reconsideration of the previously proposed model. In this work, we used Exo III footprinting to determine the translocation state of the stalled TEC. We observe a poor correlation between the translocation states of the TECs as determined by Exo III footprinting and the abundance of

the fast fraction in the EDTA quench between the different TECs formed by WT Pol II, as well as between the WT and rpb1-E1103G mutant TECs. It precludes modeling of the fast and slow fractions, observed in EDTA quench setup, as the post- and pre-translocated states of the TEC. New experimental approaches, similar to ones developed for DNA polymerases (Tsai and Johnson, 2006) and reverse transcriptase (Marchand et al., 2007) are required to understand the dynamics of NTP binding and translocation of multisubunit RNA polymerases.

Name	Sequence
NDS45C	5’ CCT ATA GGA TAC TTA CAG CCA TCG AGA GGG ACA AGG CGA AAA GAG 3’
NDS45T	5’ CCT ATA GGA TAC TTA CAG CCA TCG AGA GGG ATA AGG CGA AAA GAG 3’
NDS45G	5’ CCT ATA GGA TAC TTA CAG CCA TCG AGA GGG AGA AGG CGA AAA GAG 3’
NDS65	5’ CCT ATA GGA TAC TTA CAG CCA TCG AGA GGG ACA CGG CGA ATA CCC ATC CCA ATC GGC CTG CT/bio/G GT- 3’
NDS65C	5’ CCT ATA GGA TAC TTG GGG GCA TCG AGA GGG ACA CGG CGA ATA CCC ATC CCA ATC GGC CTG CT/bio/G GT- 3’
RNA7	5’ CGAGAGG 3’
RNA8	5’ UCGAGAGG 3’
RNA7(20)	5’ CGGCGAA 3’
RNA9	5’ AUCGAGAGG 3’

Supplementary Table. Oligonucleotides used for the TECs assembly. The sequences for the non-template (sense) DNA strands and for the RNA primers are shown. The template DNA strands are fully complementary to the non-template DNA strands.

.

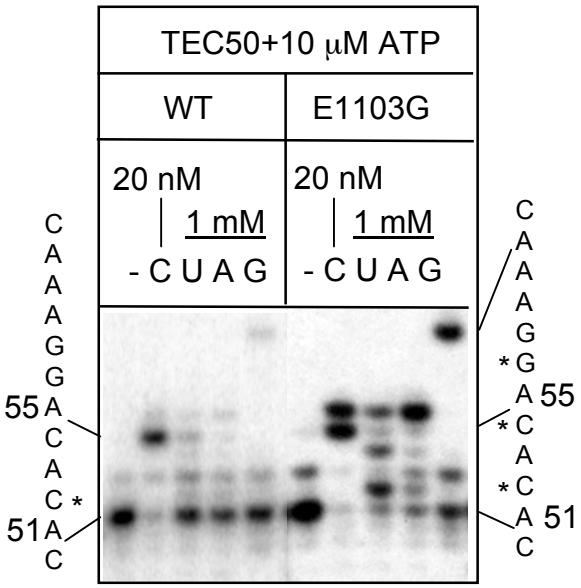

Supplementary Figure 1. E1103G substitution efficiently promotes misincorporation and mismatch extension in the TECs containing extended transcripts. 5'-end-labeled TEC9 ligated to 160-bp DNA fragment (Kireeva et al., 2005) was walked to form TEC50, and incubated with 10 μM ATP for 30 sec to form TEC51. 20 nM CTP or 1 mM UTP, GTP, or ATP were added to TEC51 for 5 min, the reaction was stopped by addition of the gel-loading buffer, and the transcription products were analyzed in a 10% denaturing polyacrylamide gel. The encoded sequence is shown at both sides, the positions were misincorporation occurs are marked by the asterisks.

A

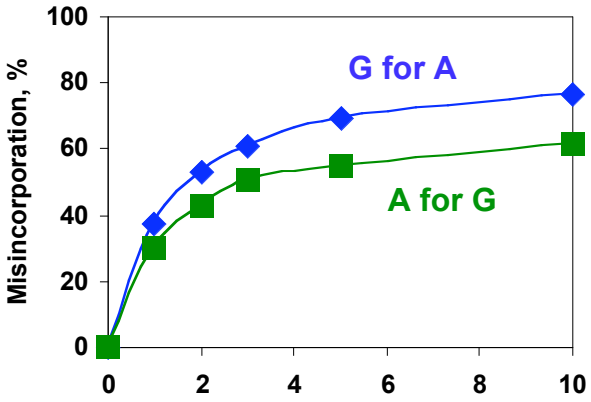

TEC9
↓ i+
…AGGGACA…

TEC9 mis-incorporates ATP for GTP
A is in *i*+2 position

TEC10
↓ i+
…AGGGACA…

TEC10 mis-incorporates GTP for ATP
C is in *i*+2 position

Prediction of the template misalignment mechanism of misincorporation :
G*(A),C < A*(G),A

Result:
G*(A),C > A*(G),A

B

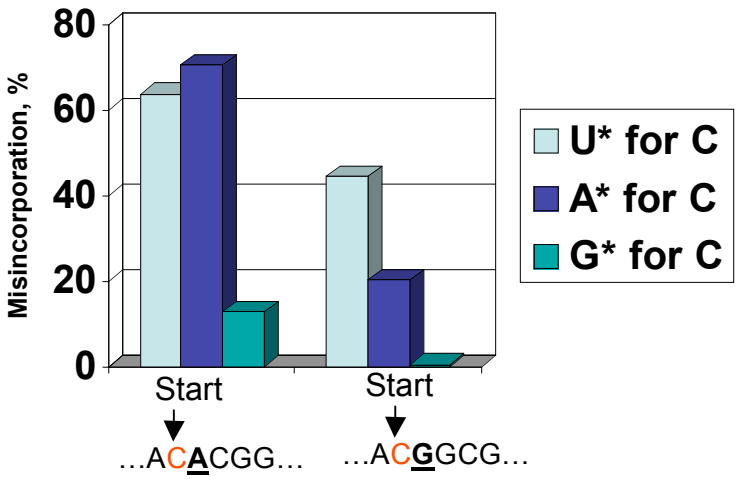

Prediction of the template misalignment mechanism of misincorporation :

A*(C),A > U*(C),A
G*(C),G > U*(C),G
A*(C),A > A*(C),G

Result:

A*(C),A = U*(C),A
G*(C),G < U*(C),G
A*(C),A > A*(C),G
G*(C),G < G*(C),A

Supplementary Figure 2. Misincorporation patterns within different sequence contexts are not fully consistent with the template misalignment mechanism of misincorporation.
A, Time-courses of GMP for AMP and AMP for GMP misincorporation. TEC9 has been assembled with RNA9 on template 45C, and incubated with 1 mM GTP or 1 mM ATP. If misincorporation occurs by template misalignment, misincorporation of AMP, followed by the correct AMP (A*(G), A), is expected to be more efficient than misincorporation of GMP, which is followed by the correct CMP (G*(A), C).
B, Misincorporation of AMP and GMP for CMP in two sequence contexts. TEC9 has been obtained by incubation of TEC7, assembled on TDS65 and NDS65 with RNA7, with ATP and GTP. TEC9 has been incubated with CTP, washed, and incubated with ATP to obtain TEC11. Misincorporation efficiency has been determined in TEC9 and TEC11 after 10 min incubation with 1 mM UTP, ATP, or GTP. If misincorporation occurs by template misalignment, transversions A*(C), A in TEC9 and G*(C), G in TEC11 are expected to be more efficient than transitions U*(C), A and U*(C), G.

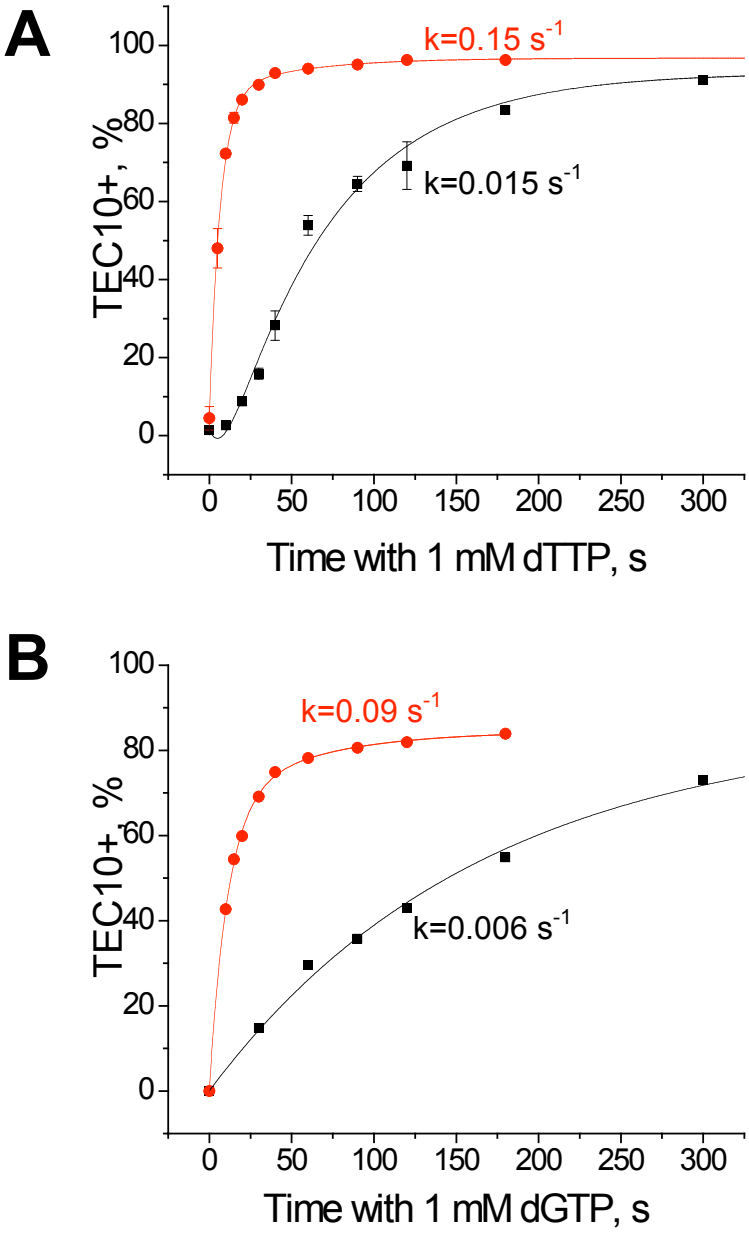

Supplementary Figure 3. E1103G mutation in Rpb1 promotes dNTP incorporation. The TECs were formed on the 45U (A) or the 45G (B) templates (see Fig. 2 for the template sequences), and incorporation of dTTP or dGTP has been analyzed as described in Fig. 3. The data in (A) are the averages of three experiments, and the error bars show standard deviation.

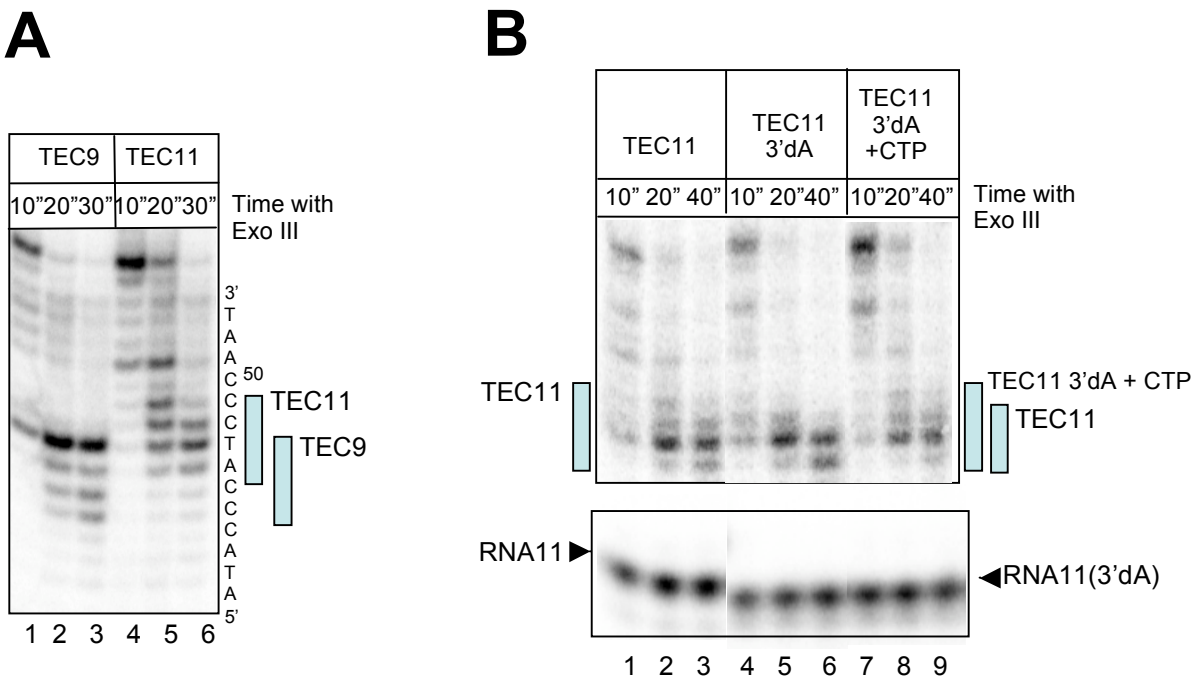

Supplementary Figure 4. Front-end boundary of WT Pol II TEC determined by Exo III footprinting. TEC11 was obtained by incubation of TEC9, assembled on TDS65 with RNA9 and non-biotinylated NDS65, with 10 μM each GTP and ATP or 10 μM each GTP and 3’dATP. Note the slightly faster mobility of RNA11 carrying 3’dAMP.

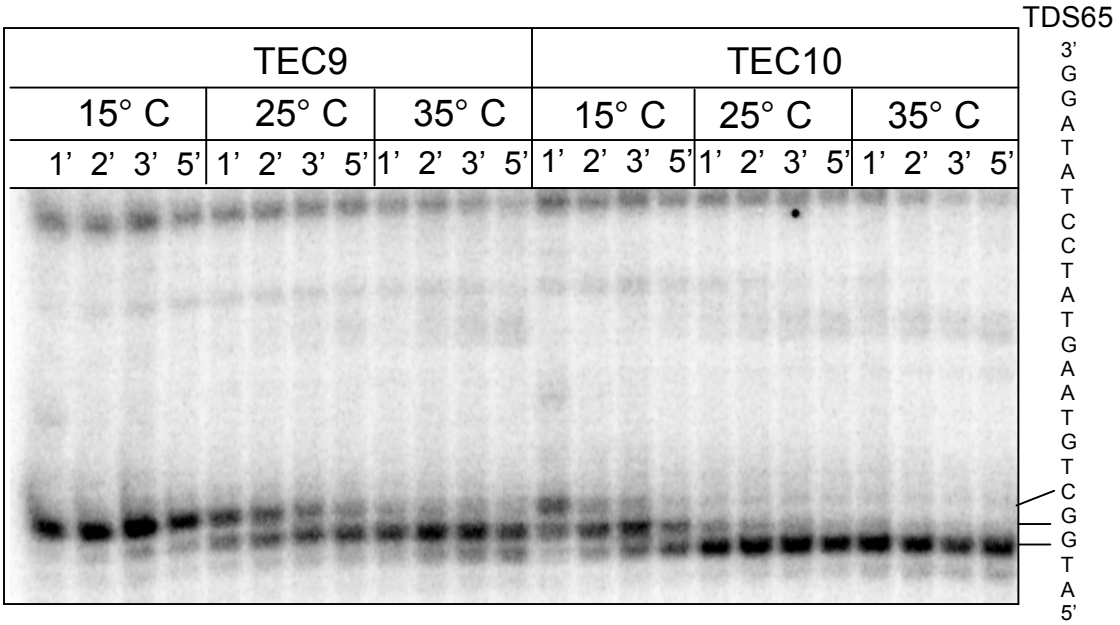

Supplementary Figure 5. Temperature dependence of the Pol II Exo III footprint. The TECs were obtained with WT Pol II as in the experiment shown in Fig. 4.

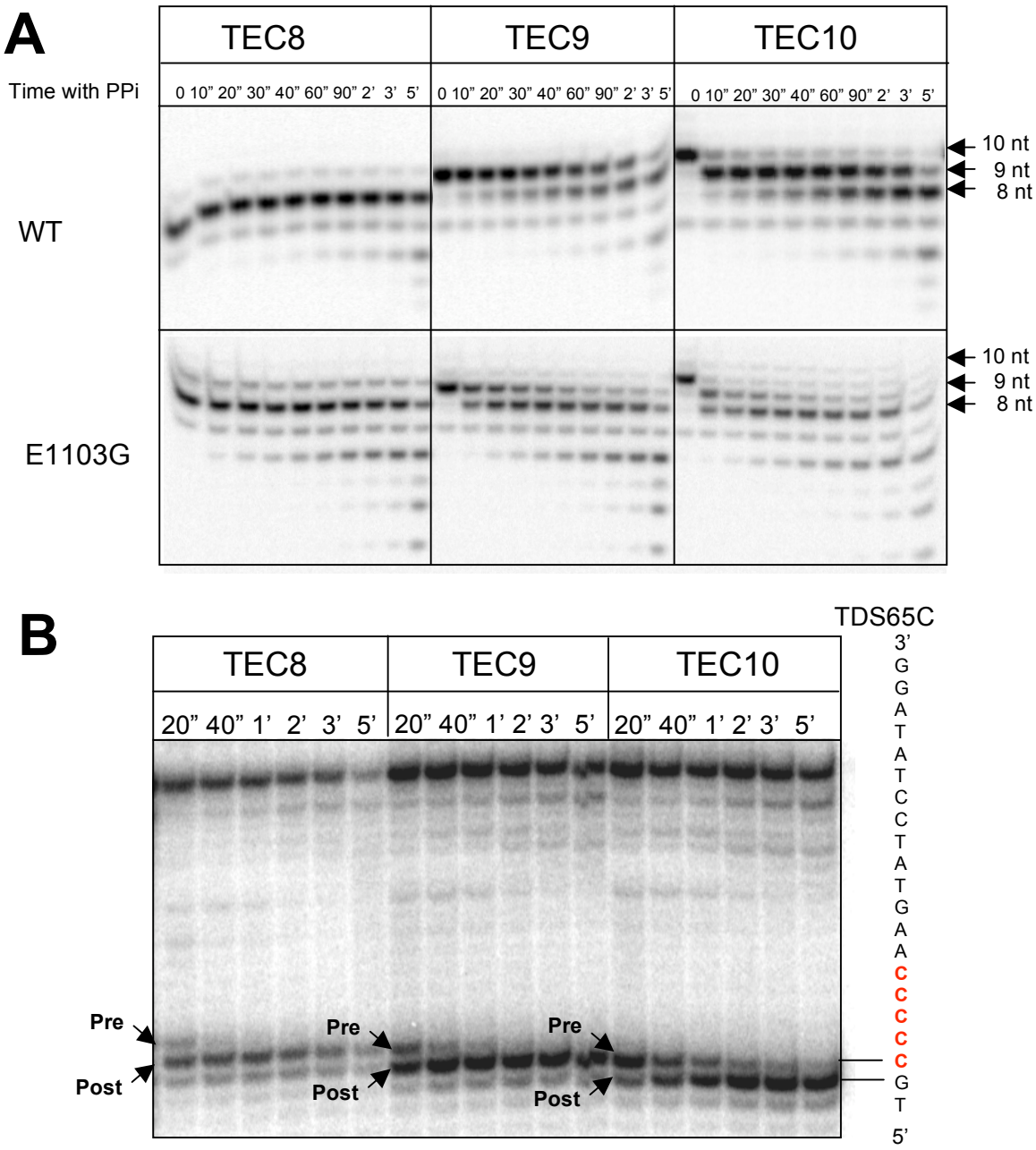

Supplementary Figure 6. Assays for the translocation state of the TECs: pyrophosphorolysis and Exo III footprinting.

A, The TECs formed by the WT (upper panel) or E1103G (lower panel) Pol II and carrying 5'-end-labeled RNAs were treated with 2 mM tetrapotassium pyrophosphate for the indicated times. The reactions were stopped with the gel-loading buffer, and the RNA products were analyzed in 20% polyacrylamide gels.

B, TEC8, 9 and 10 were obtained with WT Pol II and treated as described for the experiment shown in Fig. 4, but TDS65C and NDS65C were used instead of TDS65 and NDS65. TDS65C is derived from TDS65 by substitution of the (5' G_{46}GCTGTA$_{52}$ 3') sequence with the (5'G_{46}CCCCCA$_{52}$3') sequence. NDS65C is fully complementary to TDS65C, and biotinylated at the 3'-end.

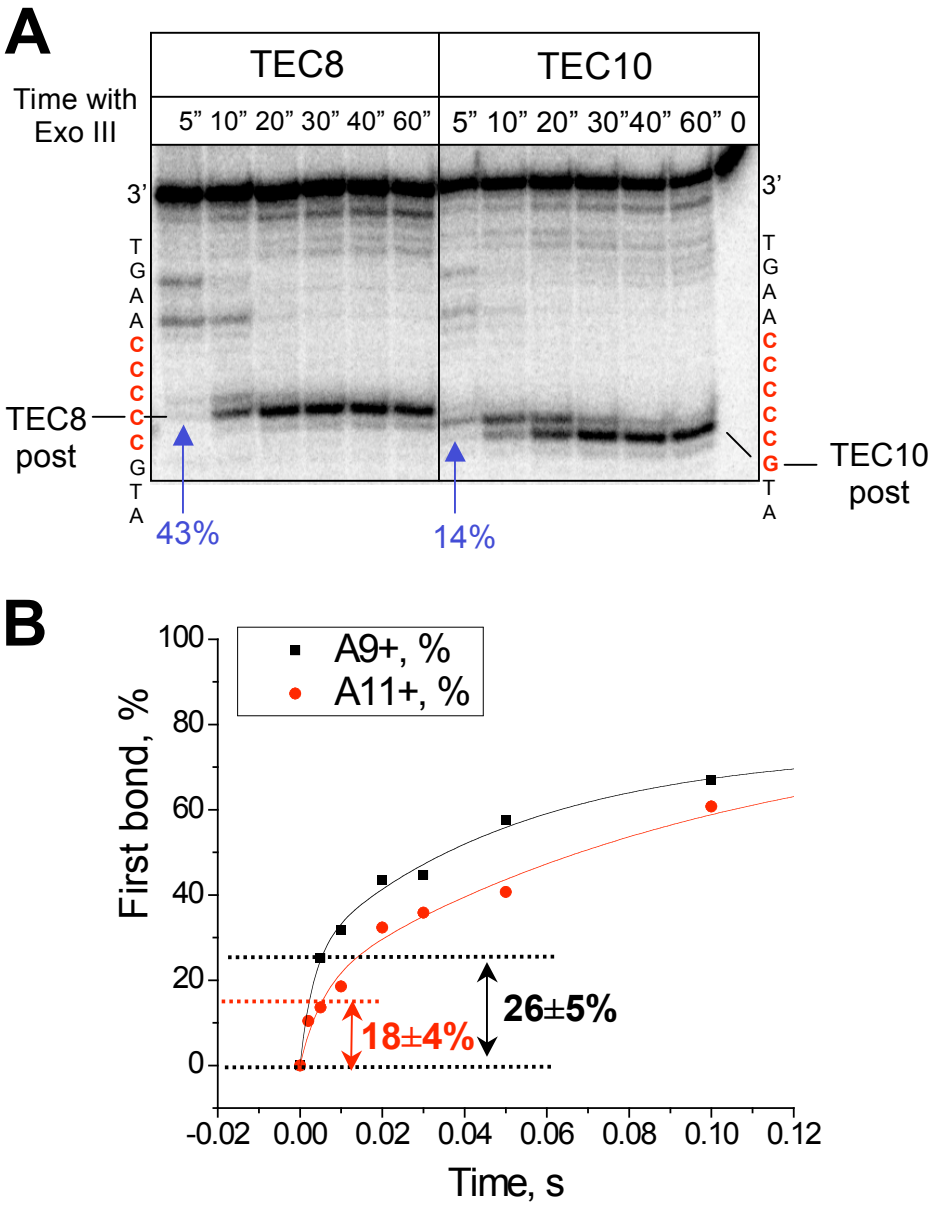

Supplementary Figure 7. Assays for the translocation state of the TECs: Exo III footprinting and resistance to EDTA.
A, the TECs were obtained as described in the legend for Fig. 4 and Supplementary Fig. 6B on TDS65C.The positions of footprints attributed to the post-translocated TECs are indicated by blue arrows. B, TEC7 was incubated with 10 μM GTP, and TEC9 was incubated with 10 μM CTP for 5 sec to obtain TEC8 and TEC10, which were subsequently chased with 1 mM each ATP and CTP. The reaction was stopped by rapid mixing with EDTA, and the percentage of the RNA extended to 9 nt (black symbols) or 11-nt (red symbols) was plotted against time. The amplitude of the fast fraction was determined by fitting each data set with a double-exponential equation (black and red lines).

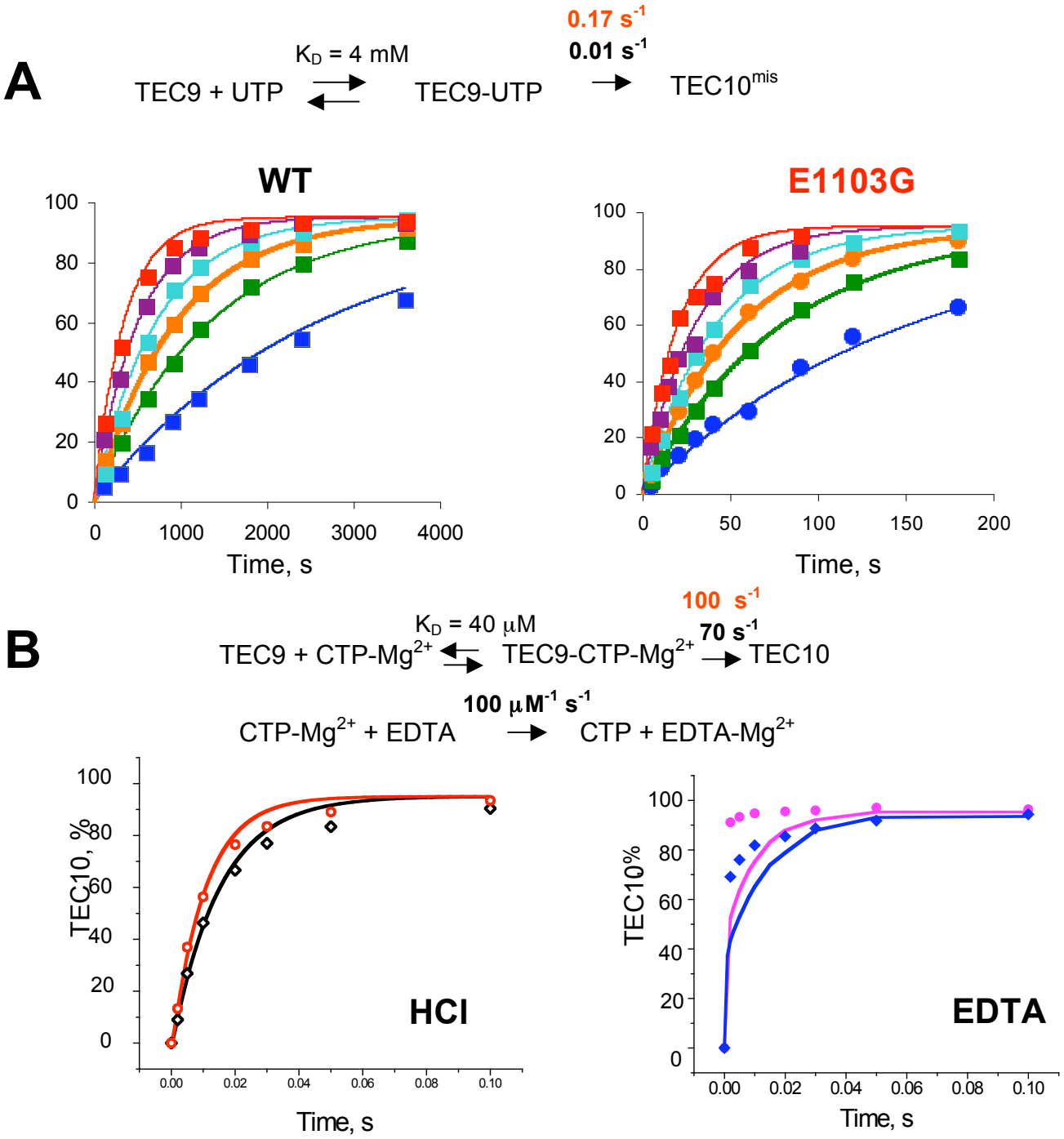

Supplementary Figure 8. Kinetic modeling of misincorporation and correct NTP incorporation data (experiment described in Fig. 5) with a two-step mechanism lacking isomerization step.
A, Fit of misincorporation data suggests a 17-fold increase of the bond formation rate in the mutant Pol II. Misincorporation has been monitored at 200 (blue), 400 (green), 600 (orange), 800 (cyan), 1200 (purple), and 2000 (red) μM UTP.
B, The two-step mechanism does not explain the results obtained with EDTA quench. The increase of the phosphoryl transfer rate accounts for the apparent increase of the TEC10 formation in the mutant (HCl quench; WT shown in black, E1103G mutant in red), but not for the increased efficiency of CTP sequestration (EDTA quench; WT shown in blue, and E1103G in magenta). CTP concentration was 1 mM.

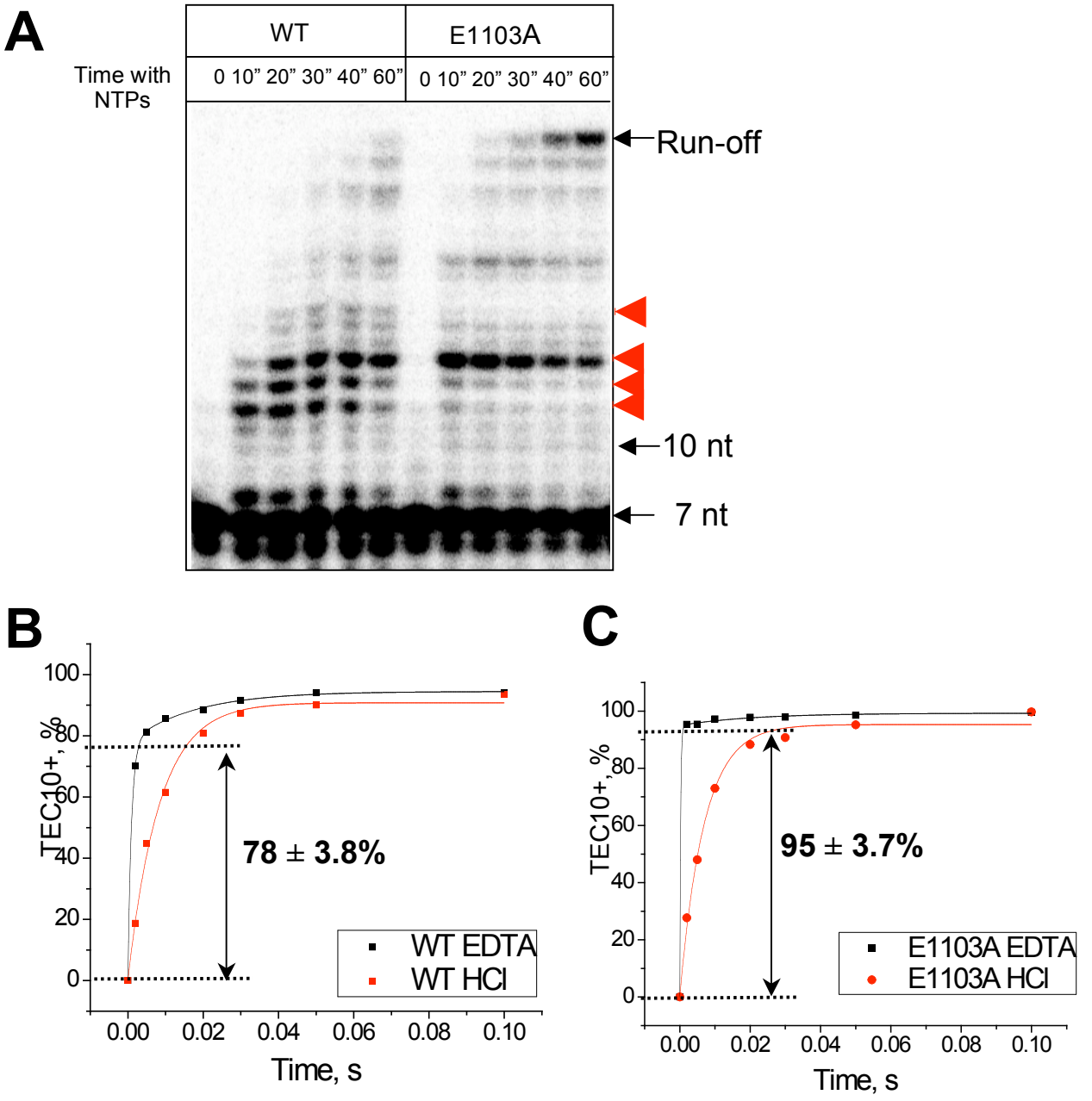

Supplementary Figure 9. Rpb1-E1103A mutation obtained by site-directed mutagenesis suppresses transcription pauses and promotes isomerization. The experiment has been done with Pol II immobilized on Ni-NTA agarose directly from the cell lysate (Kireeva et al., 2003). The *S.cerevisiae* strains encoding tagged Rpb3 and carrying chromosomal *RPB1* or *rpb1-E1103A* were grown overnight in YEPD. Cells from 6 ml culture were collected, washed with TB, and lysed by vortexing with glass beads. The lysate has been incubated with 100 μl Ni-NTA agarose pellet, and washed 3 times with TB. The elongation complex was assembled on TDS65 template hybridized to r7(20) RNA (5' ACGGCGAA 3') and NDS65, and washed 3 times with TB. The TEC was eluted with 100 mM imidazole in TB. A, TEC7 was chased with 10 μM NTPs. The reaction was stopped with addition of the gel-loading buffer after the indicated incubation time. The pause sites suppressed by the E1103A mutation are indicated by red arrowheads. The individual bond formation was analyzed for the WT (B) and E1103A (C) TECs by incubating TEC7 with 10 μM ATP and UTP for 5 sec, and chasing the resulting TEC9 with 1 mM each ATP and CTP. The reaction was stopped with EDTA or HCl. The amplitudes of the fast fraction were determined by double-exponential fit of EDTA quench data sets (black lines).

Supplementary References

Artsimovitch,I., Chu,C., Lynch,A.S., and Landick,R. (2003). A new class of bacterial RNA polymerase inhibitor affects nucleotide addition. Science *302*, 650-654.

Bar-Nahum,G., Epshtein,V., Ruckenstein,A.E., Rafikov,R., Mustaev,A., and Nudler,E. (2005). A ratchet mechanism of transcription elongation and its control. Cell *120*, 183-193.

Foster,J.E., Holmes,S.F., and Erie,D.A. (2001). Allosteric binding of nucleoside triphosphates to RNA polymerase regulates transcription elongation. Cell *106*, 243-252.

Gong,X.Q., Zhang,C., Feig,M., and Burton,Z.F. (2005). Dynamic error correction and regulation of downstream bubble opening by human RNA polymerase II. Mol. Cell *18*, 461-470.

Guo,Q. and Sousa,R. (2006). Translocation by T7 RNA polymerase: a sensitively poised Brownian ratchet. J. Mol. Biol. *358*, 241-254.

Holmes,S.F. and Erie,D.A. (2003). Downstream DNA sequence effects on transcription elongation. Allosteric binding of nucleoside triphosphates facilitates translocation via a ratchet motion. J. Biol. Chem. *278*, 35597-35608.

Holmes,S.F., Foster,J.E., and Erie,D.A. (2003). Kinetics of multisubunit RNA polymerases: experimental methods and data analysis. Methods Enzymol. *371*, 71-81.

Kashkina,E., Anikin,M., Tahirov,T.H., Kochetkov,S.N., Vassylyev,D.G., and Temiakov,D. (2006). Elongation complexes of Thermus thermophilus RNA polymerase that possess distinct translocation conformations. Nucleic Acids Res. *34*, 4036-4045.

Kireeva,M.L., Hancock,B., Cremona,G.H., Walter,W., Studitsky,V.M., and Kashlev,M. (2005). Nature of the nucleosomal barrier to RNA polymerase II. Mol. Cell *18*, 97-108.

Kireeva,M.L., Lubkowska,L., Komissarova,N., and Kashlev,M. (2003). Assays and affinity purification of biotinylated and nonbiotinylated forms of double-tagged core RNA polymerase II from Saccharomyces cerevisiae. Methods Enzymol. *370*, 138-155.

Komissarova,N. and Kashlev,M. (1997). RNA polymerase switches between inactivated and activated states By translocating back and forth along the DNA and the RNA. J. Biol. Chem. *272*, 15329-15338.

Komissarova,N. and Kashlev,M. (1998). Functional topography of nascent RNA in elongation intermediates of RNA polymerase. Proc. Natl. Acad. Sci. U. S. A *95*, 14699-14704.

Landick,R. and Yanofsky,C. (1987). Isolation and structural analysis of the Escherichia coli trp leader paused transcription complex. J. Mol. Biol. *196*, 363-377.

Linxweiler,W. and Horz,W. (1982). Sequence specificity of exonuclease III from E. coli. Nucleic Acids Res. *10*, 4845-4859.

Marchand,B., Tchesnokov,E.P., and Gotte,M. (2007). The pyrophosphate analogue foscarnet traps the pre-translocational state of HIV-1 reverse transcriptase in a Brownian ratchet model of polymerase translocation. J. Biol. Chem. *282*, 3337-3346.

Metzger,W., Schickor,P., and Heumann,H. (1989). A cinematographic view of Escherichia coli RNA polymerase translocation. EMBO J. *8*, 2745-2754.

Nedialkov,Y.A., Gong,X.Q., Hovde,S.L., Yamaguchi,Y., Handa,H., Geiger,J.H., Yan,H., and Burton,Z.F. (2003a). NTP-driven translocation by human RNA polymerase II. J. Biol. Chem. *278*, 18303-18312.

Nedialkov,Y.A., Gong,X.Q., Yamaguchi,Y., Handa,H., and Burton,Z.F. (2003b). Assay of transient state kinetics of RNA polymerase II elongation. Methods Enzymol. *371*, 252-264.

Nudler,E., Goldfarb,A., and Kashlev,M. (1994). Discontinuous mechanism of transcription elongation. Science *265*, 793-796.

Samkurashvili,I. and Luse,D.S. (1996). Translocation and transcriptional arrest during transcript elongation by RNA polymerase II. J. Biol. Chem. *271*, 23495-23505.

Toulokhonov,I., Zhang,J., Palangat,M., and Landick,R. (2007). A central role of the RNA polymerase trigger loop in active-site rearrangement during transcriptional pausing. Mol. Cell *27*, 406-419.

Tsai,Y.C. and Johnson,K.A. (2006). A new paradigm for DNA polymerase specificity. Biochemistry *45*, 9675-9687.

Zhang,C. and Burton,Z.F. (2004). Transcription factors IIF and IIS and nucleoside triphosphate substrates as dynamic probes of the human RNA polymerase II mechanism. J. Mol. Biol. *342*, 1085-1099.

Zhang,C., Yan,H., and Burton,Z.F. (2003). Combinatorial control of human RNA polymerase II (RNAP II) pausing and transcript cleavage by transcription factor IIF, hepatitis delta antigen, and stimulatory factor II. J. Biol. Chem. *278*, 50101-50111.